



**HAL**  
open science

## **Vitamin D Receptor Antagonist MeTC7 Inhibits PD-L1**

Negar Khazan, Emily Quarato, Niloy Singh, Cameron Snyder, Taylor Moore, John Miller, Masato Yasui, Yuki Teramoto, Takuro Goto, Sabeeha Reshi, et al.

► **To cite this version:**

Negar Khazan, Emily Quarato, Niloy Singh, Cameron Snyder, Taylor Moore, et al.. Vitamin D Receptor Antagonist MeTC7 Inhibits PD-L1. *Cancers*, 2023, 15 (13), pp.3432. 10.3390/cancers15133432 . hal-04274207

**HAL Id: hal-04274207**

**<https://hal.science/hal-04274207>**






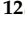



Submitted on 7 Nov 2023

**HAL** is a multi-disciplinary open access archive for the deposit and dissemination of scientific research documents, whether they are published or not. The documents may come from teaching and research institutions in France or abroad, or from public or private research centers.

L'archive ouverte pluridisciplinaire **HAL**, est destinée au dépôt et à la diffusion de documents scientifiques de niveau recherche, publiés ou non, émanant des établissements d'enseignement et de recherche français ou étrangers, des laboratoires publics ou privés.

## Article

# Vitamin D Receptor Antagonist MeTC7 Inhibits PD-L1

Negar Khazan <sup>1</sup>, Emily R. Quarato <sup>2</sup>, Niloy A. Singh <sup>1</sup>, Cameron W. A. Snyder <sup>1</sup>, Taylor Moore <sup>1</sup>, John P. Miller <sup>1,3</sup>, Masato Yasui <sup>4</sup>, Yuki Teramoto <sup>4</sup>, Takuro Goto <sup>4</sup>, Sabeeha Reshi <sup>5</sup>, Jennifer Hong <sup>5</sup>, Naixin Zhang <sup>1</sup>, Diya Pandey <sup>1</sup>, Priyanka Srivastava <sup>1</sup>, Alexandra Morell <sup>1</sup>, Hiroki Kawano <sup>6</sup>, Yuko Kawano <sup>6</sup>, Thomas Conley <sup>6</sup>, Deepak M. Sahasrabudhe <sup>6</sup>, Naohiro Yano <sup>7</sup>, Hiroshi Miyamoto <sup>4</sup>, Omar Aljitiawi <sup>6</sup>, Jane Liesveld <sup>6</sup>, Michael W. Becker <sup>6</sup>, Laura M. Calvi <sup>6</sup>, Alexander S. Zhovmer <sup>8</sup>, Erdem D. Tabdanov <sup>9</sup>, Nikolay V. Dokholyan <sup>10</sup>, David C. Linehan <sup>11</sup>, Jeanne N. Hansen <sup>12</sup>, Scott A. Gerber <sup>13,14</sup>, Ashoke Sharon <sup>15</sup>, Manoj K. Khera <sup>16</sup>, Peter W. Jurutka <sup>5,17,\*</sup>, Natacha Rochel <sup>18</sup>, Kyu Kwang Kim <sup>1</sup>, Rachael B. Rowswell-Turner <sup>1</sup>, Rakesh K. Singh <sup>1,\*</sup> and Richard G. Moore <sup>1</sup>

- <sup>1</sup> Wilmut Cancer Institute and Division of Gynecologic Oncology, Department of Obstetrics and Gynecology, University of Rochester Medical Center, Rochester, NY 14642, USA; alexandra\_morell@urmc.rochester.edu (A.M.); kyukwang\_kim@urmc.rochester.edu (K.K.K.); richard\_moore@urmc.rochester.edu (R.G.M.)
- <sup>2</sup> Department of Environmental Medicine, University of Rochester Medical Center, Rochester, NY 14642, USA
- <sup>3</sup> Department of Microbiology and Immunology, University of Rochester Medical Center, Rochester, NY 14642, USA
- <sup>4</sup> Department of Pathology and Laboratory Medicine, University of Rochester Medical Center, Rochester, NY 14642, USA; yabomabo@gmail.com (M.Y.)
- <sup>5</sup> School of Mathematical and Natural Sciences, University of Arizona College of Medicine, Phoenix, AZ 85004, USA
- <sup>6</sup> Department of Medicine, Hematology/Oncology, University of Rochester Medical Center, Rochester, NY 14642, USA; thomas\_conely@urmc.rochester.edu (T.C.)
- <sup>7</sup> Division of Surgical Research, Rhode Island Hospital, Brown University, Providence, RI 02912, USA; naohiro\_yano@brown.edu
- <sup>8</sup> Center for Biologics Evaluation and Research, U.S. Food and Drug Administration, Silver Spring, MD 20993, USA
- <sup>9</sup> CytoMechanobiology Laboratory, Department of Pharmacology, Penn State College of Medicine, Pennsylvania State University, Hershey, PA 17033, USA
- <sup>10</sup> Department of Pharmacology, Department of Biochemistry & Molecular Biology, Center for Translational Systems Research, Penn State College of Medicine, Pennsylvania State University, Hershey, PA 17033, USA; nxd338@psu.edu
- <sup>11</sup> Division of Surgery, University of Rochester Medical Center, Rochester, NY 14642, USA
- <sup>12</sup> Department of Psychological and Brain Sciences, Colgate University, Hamilton, NY 13346, USA
- <sup>13</sup> Division of Surgery and Microbiology and Immunology, University of Rochester Medical Center, Rochester, NY 14642, USA
- <sup>14</sup> Department of Radiation Oncology, University of Rochester Medical Center, Rochester, NY 14642, USA
- <sup>15</sup> Birla Institute of Technology, Ranchi 835215, India
- <sup>16</sup> Presude Lifesciences, Delhi 110075, India
- <sup>17</sup> School of Mathematical and Natural Sciences, Arizona State University, Health Futures Center, Phoenix, AZ 85054, USA
- <sup>18</sup> Institute of Genetics and of Molecular and Cellular Biology, 67400 Illkirch-Graffenstaden, France
- \* Correspondence: peter.jurutka@asu.edu (P.W.J.); rakesh\_singh@urmc.rochester.edu (R.K.S.); Tel.: +1-602-543-6087 (P.W.J.); +1-585-276-6281 (R.K.S.)



**Citation:** Khazan, N.; Quarato, E.R.; Singh, N.A.; Snyder, C.W.A.; Moore, T.; Miller, J.P.; Yasui, M.; Teramoto, Y.; Goto, T.; Reshi, S.; et al. Vitamin D Receptor Antagonist MeTC7 Inhibits PD-L1. *Cancers* **2023**, *15*, 3432. <https://doi.org/10.3390/cancers15133432>

Academic Editors: Mario Roselli, Patrizia Ferroni and Fiorella Guadagni

Received: 10 June 2023  
Revised: 27 June 2023  
Accepted: 28 June 2023  
Published: 30 June 2023



**Copyright:** © 2023 by the authors. Licensee MDPI, Basel, Switzerland. This article is an open access article distributed under the terms and conditions of the Creative Commons Attribution (CC BY) license (<https://creativecommons.org/licenses/by/4.0/>).

**Simple Summary:** Programmed death-ligand 1 (PD-L1) enables immune evasion of tumors. Antibodies targeting PD-L1/PD-1 exhibit durable responses in eligible patients. However, antibodies cause life-threatening toxicities. Small molecules targeting PD-L1, or the drivers of PD-L1 or PD-L1/PD-1 axis, are being explored as alternatives. Thus, identifying vitamin D/vitamin D receptor (VDR) as the driver of PD-L1 expression in AML significantly enhances our understanding of the origin of PD-L1-driven immune evasions in AML and malignancies of pancreas and ovaries, where similar transcriptional regulation has been observed. To target vitamin D/VDR, we have developed MeTC7, which inhibits PD-L1 expression in vitro and in vivo and provides a new approach to block PD-L1/PD-1-driven tumorigenesis.

**Abstract:** Small-molecule inhibitors of PD-L1 are postulated to control immune evasion in tumors similar to antibodies that target the PD-L1/PD-1 immune checkpoint axis. However, the identity of targetable PD-L1 inducers is required to develop small-molecule PD-L1 inhibitors. In this study, using chromatin immunoprecipitation (ChIP) assay and siRNA, we demonstrate that vitamin D/VDR regulates PD-L1 expression in acute myeloid leukemia (AML) and myelodysplastic syndrome (MDS) cells. We have examined whether a VDR antagonist, MeTC7, can inhibit PD-L1. To ensure that MeTC7 inhibits VDR/PD-L1 without off-target effects, we examined competitive inhibition of VDR by MeTC7, utilizing ligand-dependent dimerization of VDR-RXR, RXR-RXR, and VDR-coactivators in a mammalian 2-hybrid (M2H) assay. MeTC7 inhibits VDR selectively, suppresses PD-L1 expression sparing PD-L2, and inhibits the cell viability, clonogenicity, and xenograft growth of AML cells. MeTC7 blocks AML/mesenchymal stem cells (MSCs) adhesion and increases the efferocytotic efficiency of THP-1 AML cells. Additionally, utilizing a syngeneic colorectal cancer model in which VDR/PD-L1 co-upregulation occurs in vivo under radiation therapy (RT), MeTC7 inhibits PD-L1 and enhances intra-tumoral CD8<sup>+</sup>T cells expressing lymphoid activation antigen-CD69. Taken together, MeTC7 is a promising small-molecule inhibitor of PD-L1 with clinical potential.

**Keywords:** PD-L1; AML; MDS; vitamin D; VDR; small molecule; M2H assay; efferocytosis

## 1. Introduction

The programmed death-ligand-1 (PD-L1)/programmed cell death protein-1 (PD-1) axis is a well-characterized immune evasion mechanism of tumors [1,2]. Several other checkpoint molecules, such as CTLA-4 [3] and V-domain Ig suppressor of T-cell activation (VISTA) [4], are also involved in the immune escape of tumors. Drivers of PD-L1 expression on tumor cells have been identified [5,6]. Calcitriol, the active form of vitamin D, was shown to upregulate PD-L1 in AML and head/neck cancer cell lines [7]. Phorbol esters, retinoic acid, and interferon-gamma also regulate PD-L1 expression in tumor cells [8–10].

Monoclonal antibodies targeting the PD-L1/PD-1 axis have shown lasting responses in melanoma and carcinomas of the breast, bladder, cervix, uterus, and lung [11]. A portion of cancer patients do not benefit from PD-L1/PD-1 targeted immunotherapies [12]. In addition, monoclonal antibodies cause life-threatening immune adverse reactions, face resistance, and carry poor pharmacodynamics, e.g., the inability to penetrate tumors and inhibit intracellular or exosomal PD-L1 [13]. The intracellular reservoir of PD-L1 can rebound to cell membranes and reduce immunotherapy outcomes [14]. Similarly, exosomal PD-L1 can promote immune tolerance and negate immunotherapy outcomes [15,16]. Further, secreted splice variants of PD-L1 can entrap PD-L1 targets in antibody therapies limiting their effectiveness [17].

There is a growing interest in the development of small molecules that can inhibit PD-L1 or block PD-L1/PD-1 interactions similar to antibodies [18–22]. Examples of the leading small-molecule inhibitors of the PD-L1/PD-1 axis include BMS202, CA-170, and INCB086550 [18–23]. Identifying small-molecule inhibitors of PD-L1 is impaired by: (1) the flat topology of PD-L1, which impairs small molecules' ability to dock, and (2) the lack of the identity of drug-responsive regulators of PD-L1 [10]. We and Dimitrov et al. [7] have identified vitamin D/VDR as a drug-responsive driver of PD-L1 in AML, MDS, and ovarian and pancreatic cancer cells. Targeting VDR is challenged by the unavailability of pharmacologically pure antagonists. Recently, we described the identification of MeTC7, a pharmacologically pure VDR antagonist [24].

In this study, we aim to investigate the mechanism of VDR inhibition using a mammalian 2-hybrid (M2H) assay to validate its actions against VDR and dimerization of VDR-RXR, an obligatory step in the activation of VDR signaling. Furthermore, we aim to examine whether antagonist binding also blocks the formation of VDR complexes with essential coactivators (SRC, DRIP205) needed for gene inductions by VDR. Next, we aimed to examine whether MeTC7 can inhibit PD-L1 expression in a panel of diverse tumor

cell types (AML, ovarian and pancreatic cancer) *in vitro* and in a syngeneic model that converges overexpression of both VDR/PD-L1 under the same settings. Taken together, this study deepens our understanding of the pharmacologic mechanism of actions of MeTC7 and presents it as a promising small-molecule inhibitor of PD-L1.

## 2. Materials and Methods

**Study design:** VDR overexpression in AML subtypes and its impact on survival will be determined by analysis of AMPL patients' microarray databases (Bloodspot and R2-Genomics and Visualization platform). The association of vitamin D/VDR with PD-L1 will be validated by a CHIP assay and siRNA knockdown of VDR. The mechanism of VDR antagonism of MeTC7 will be examined by M2H assay. PD-L1 expression in MeTC7-treated primary AML or cell lines will be examined by immunoblotting. The effects of MeTC7 on the viability and clonogenicity of AML will be examined by MTS assay, colony counts, and microscopy. The adhesion of AML cells with mesenchymal stem cells will be examined by co-culture experiments. The effect of MeTC7 on efferocytosis will be examined by co-culture of THP-1 cells with apoptosed neutrophils. *In vivo* anti-PD-L1 activity will be examined by a syngeneic mouse colon cancer model.

**Collection of untreated and relapsed AML cells:** Primary AML, relapsed AML, and bone marrow (BM) cells were isolated from AML patients and healthy donors who had provided their informed consent at the University of Rochester Medical Center.

**VDR expression in human AML and correlation with survival:** VDR mRNA expression in AML subtypes versus normal hematopoietic stem cells (HSC) controls were established via analysis of the Bloodspot database of AML patients comparing to normal hematopoiesis ([https://servers.binf.ku.dk/bloodspot/?gene=VDR&dataset=normal\\_human\\_v2\\_with\\_AMLs](https://servers.binf.ku.dk/bloodspot/?gene=VDR&dataset=normal_human_v2_with_AMLs) (accessed on 26 June 2023)). The association of VDR mRNA overexpression with survival in AML patients was analyzed using the R2-Genomics.org platform (Database: Bohlander\_422-Mas5.0-u13a; <https://hgserver1.amc.nl/cgi-bin/r2/main.cgi> (accessed on 26 June 2023)). The system-selected VDR mRNA expression cut-off was set to 70.8. The expression of VDR and PD-L1 proteins in cultured AML primary cells and cell lines was analyzed using Western blot, as described previously [24].

**Cell lines and MeTC7:** AML cell lines (MOLM13, MV411, THP1, and U937) purchased from American Type Culture Collection (ATCC, Manassas, VA) were cultured in RPMI medium (Gibco, cat #22400) supplemented with 10% fetal bovine serum (FBS) (Hyclone, #SH30396.03) and 1% pen-strep (Gibco, cat#15140122).

**Chromatin Immunoprecipitation (ChIP):** ChIP assay was performed using the Magna ChIP kit (Millipore; #17-10085) according to the manufacturer's instructions. The detailed method of ChIP assay is described in the Supplementary Materials section.

**siRNA knockdown of VDR:** Stable VDR knockdown in AML cell lines was carried out using siRNA. Methods for siRNA knockdown are described in the Supplementary Materials section.

**Mammalian-2-hybrid (M2H) assay:** Human embryonic kidney cells (HEK293) purchased from ATCC were used to perform the mammalian-2-hybrid assays (M2H). The cells were seeded in a 24-well plate at a density of 70,000 cells/well in DMEM (Hyclone, Logan, UT, USA) supplemented with 10% FBS (Atlanta Biologicals, Flowery Branch, GA, USA), 100 µg/mL streptomycin, 100 U/mL penicillin (Caisson labs, Smithfield, UT, USA) 22–24 h prior to transfection were transiently transfected using Polyethylenimine (PEI) (Santa Cruz Biotechnology, Dallas, TX, USA) according to the manufacturer's protocol. The cells in each well received 20 ng of bait vectors and prey vectors, 250 ng of the luciferase reporter plasmid (pFR-luc), and 20 ng of pRL-null renilla control plasmid along with 1.25 µL of PEI reagent. After 22–24 h of transfection, the cells were treated with reference compound (i.e., 1,25D) either alone or in combination with MeTC7. For the RXR-RXR assay, the cells were treated with reference compound (i.e., bexarotene) and/or MeTC7. All compounds were solubilized in ethanol except MeTC7, which was solubilized in DMSO. After 24 h of treatment, the cells were harvested into 5X cell lysis buffer, and the whole cell lysates were collected and quantified for transcriptional activity using the Dual Luciferase Assay

System (Promega, Madison, WI, USA) in a Sirius FB12 luminometer (Berthold Detection Systems, Pforzheim, Germany).

MTS assay, Western blot, and colony formation assays: Cell viabilities and Western blot analyses were performed as published previously [24]. Details of the antibodies (source and catalog numbers) are described in the Materials and Methods section. Methods for estimation of colony formation in control versus MeTC7 cells are described in detail in the Supplementary Materials section. Image J software (ImageJ 1.53 t, Java 1.8.0\_322 (64-bit)) was employed for the densitometric analysis of Western blot images. Original scans of the Western blot images described in the report are provided in Figures S3 and S5.

Co-culture of mesenchymal stem cells (MSCs) with primary cells: MSCs were isolated from the low-density bone marrow and were co-cultured with AML primary cells in 8-well glass chamber slides following the methods published previously [25]. Details of the isolation and co-culture are described in the Supplementary Materials and Methods section. Cells from both the control and MeTC7-treated populations were imaged at  $200\times$  ( $20\times$  objective,  $10\times$  ocular) magnification. Image analysis was executed by a single analyst to maintain sampling consistency. AML cells stained with CellTracker Green (Thermo Fisher, Cat# C7025) were counted manually. For area quantification, ImageJ (Fiji) software was used. A total of 400 randomly selected AML cells from each population were manually traced to ensure accuracy, and as such subsequent statistical analyses were executed using  $n = 400$  for each respective population. The area of traced cell was calculated by software calibrated to image parameters. Cell viability dye intensity was determined semi-quantitatively, determining color expression via reciprocal intensity and analyzing the same 400 randomly selected cells of each population as described previously.

Efferocytosis assay: THP-1 cells seeded at  $1 \times 10^5$  density in a 24-well plate in RPMI + 10% FBS + 1% pen-strep were treated with MeTC7 (340  $\mu$ L) or vehicle for 48 h. Neutrophils were isolated from human peripheral blood (under IRB approval) via Mono-Poly resolving medium according to the manufacturer's instructions and incubated at  $-80^\circ\text{C}$  in FBS + 10% DMSO for a minimum of 24 h to induce apoptosis. Apoptotic neutrophils were washed with PBS and fluorescently labeled with 2  $\mu$ M PKH26GL (Sigma-Aldrich, Saint Louis, MO, USA, # PKH26GL-1KT) according to the manufacturer's instructions. End-stage neutrophils were then provided in excess (10:1) to plated THP-1 cells for 3 h. Cells were then imaged and collected for flow cytometry analysis. All samples were run on an LSRII flow cytometer using FSC, SSC, 355 nm (DAPI), and 535 nm (PKH26) (BD Biosciences, Franklin Lakes, NJ, USA). Analysis was performed using FlowJo version 10.7.1.

Syngeneic colorectal cancer model: MC38 cells ( $1 \times 10^5$ /mice) derived from murine colonic adenocarcinoma were injected intramuscularly in the left legs of female C57BL/6J. Mice were locally irradiated using a 3200 Curie-sealed  $^{137}\text{Cesium}$  source that operates at roughly 1.90 Gy/min, 7 days after tumor cell injection [26]. Jigs were constructed and designed to specifically treat the tumor-bearing leg with 15 Gy radiations. This source and the collimators used are calibrated periodically to ensure equal distribution of radiation. Standard calipers were used to measure tumor growth as described previously. Tumor-bearing mice were administered 25 mg/kg of MeTC7 or vehicle control (40% Hydroxypropyl-beta-cyclodextrin (Acros Organics, Geel, Belgium, # 1695740) + solutol HS15 (Sigma, San Francisco, CA, USA, # 42966) in sterile water) subcutaneously 1X/day starting 2 days before irradiation for the indicated duration of treatment.

U937 xenograft assay: U937 cells (5 million/mice) were mixed in 1:1 cold Matrigel:RPMI medium and injected subcutaneously in NSG mice. After a week, mice were treated with 10 mg/kg/IP (M-F), and tumors were measured in terms of length and width every 3 days.

Statistical analysis: The number of CFUs in the treatment versus control groups was analyzed by non-parametric *t*-test using GraphPad Prism 8.4.0 or earlier.

### 3. Results

VDR is overexpressed in AML subtypes and predicts poor prognosis: Patients with AML *inv(16)/t(16;16)*, complex AML, or *t(11q23)/MLL* exhibited significantly elevated VDR mRNA



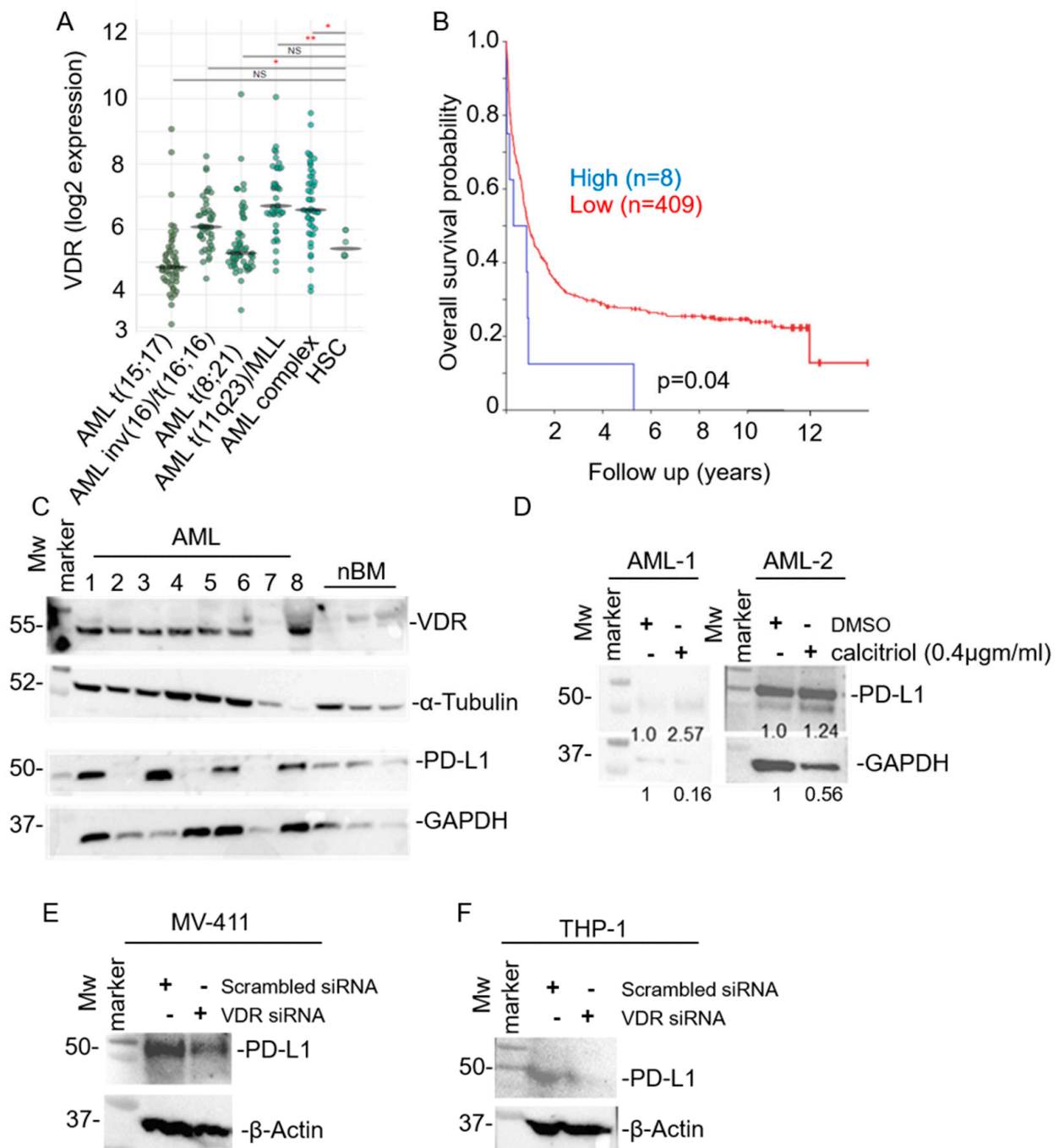
expression than hematopoietic stem cells (HSC) controls (Figure 1A). Kaplan–Meier analysis showed that AML patients overexpressing VDR ( $n = 8$ ) face increased mortalities than those with lower expression ( $n = 409$ ) ( $p = 0.04$ ) (Figure 1B). Western blot analysis of primary and relapsed AML cells (except patient 7) showed elevated VDR expression compared with normal bone marrow cells (Figure 1C). About half of the AML patient samples showed high PD-L1 expression (Figure 1C). Similarly, although not significant, PD-L1 mRNA overexpression indicated the trend for increased mortalities in AML patients (Figure S1).

VDR induces PD-L1 expression in AML and ovarian cancer cells: Calcitriol treatment induced upregulation of PD-L1 in primary AML (AML-1 and AML-2) cells (Figure 1D). Similarly, siRNA knockdown of VDR in MV411 (Figure 1E) and THP-1 (Figure 1F) cells, compared to scrambled siRNA controls, showed decreased PD-L1 expression. Original scans of the Western blots are presented in Figure S2.

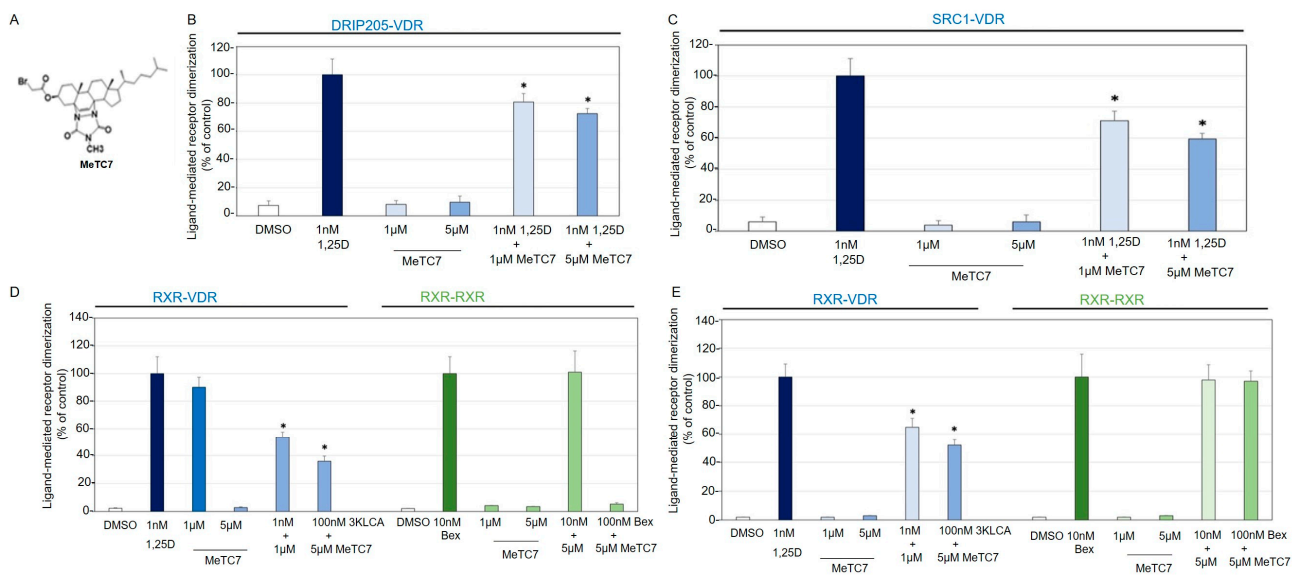
VDR/vitamin D receptor response element (VDRE) interactions in PD-L1 promoter: ChIP assay (Figure S2A) was performed following the method published by Dimitrov et al. [7] to determine VDR's interaction with PD-L1 promoter. VDR/VDRE expression in the transcripts was captured by a VDR antibody in AML (Figure S2B) and myelodysplastic syndrome (MDS) (Figure S2C). In all these cell lines examined, the PCR products for the binding site could be visualized from those precipitated by the VDR antibody. Dimitrov et al. [7] showed vitamin D/VDR regulation on PD-L1 in THP-1 AML cells. We determined that similar to THP-1 cells, MV-411 and U937 also exhibit vitamin D/VDR upregulation on PD-L1. Importantly, (MDS), a precursor to AML, also showed vitamin D/VDR regulation of PD-L1. MDS are a rare group of bone marrow failure disorders, a portion of which converts into AML.

STAT3 inhibitor does not block calcitriol-induced PD-L1 expression in THP1 AML cells: In AML and MDS, STAT3 serves as a pro-leukemogenic transcription factor that is associated with poor prognosis and short disease-free survival [27]. STAT isoforms (1, 2, 3, and 5) are situated on the promoter of PD-L1 (Figure S2A). We examined whether the pretreatment with Stattic, a characterized inhibitor of STAT3, could block calcitriol-induced PD-L1 expression. Stattic pretreatment for 6 h did not block calcitriol-induced PD-L1 upregulation; instead, increased PD-L1 expression was observed (Figure S4), indicating that vitamin D/VDR regulation of PD-L1 is Stat-3 independent.

MeTC7 is a specific VDR antagonist: The heterodimerization of RXR and VDR (RXR-VDR) and homodimerization of RXR (RXR-RXR) in an M2H demonstrated competitive inhibition by a VDR antagonist MeTC7 (Figure 2A) of only VDR-RXR heterodimers but not RXR-RXR homodimers, indicating the selective nature of the association of MeTC7 with VDR (Figure 2B). MeTC7 also demonstrated specific VDR inhibition when combined with 1,25D but did not compete nor bind with non-VDR receptors like RXR under any of the concentrations tested. Heterodimerization of VDR with transcriptional coactivators, SRC1 (Figure 2C) and DRIP205 (Figure 2D), was also effectively inhibited by MeTC7 at multiple concentrations. MeTC7 also exhibited selective competitive inhibition of VDR binding to the now-recognized alternative VDR agonist 3-keto lithocholate (3-K LCA, Figure 2E). This latter observation suggests that MeTC7 binds in the VDR ligand-binding pocket in such a way as to exclude two different natural VDR ligands (1,25D and 3-K LCA).



**Figure 1.** VDR is upregulated in AML subtypes and shows poor prognostication and upregulation of PD-L1 upon calcitriol stimulation. \*  $p < 0.05$ ; \*\*  $p < 0.01$ ; (A) The VDR mRNA expression in AML patients and survival probability were analyzed using R2-Genomics Analysis and Visualization Platform (Bohlander-422-MAS5.0\_u133a). (B) Overall survival in AML patients based on VDR expression (high:  $n = 8$ ; low:  $n = 409$ ) showed decreased survival. (C) Immunoblotting of VDR and PD-L1 in cells from randomly selected primary ( $n = 5$ ) and relapsed ( $n = 2$ ) AML patients, compared to normal bone marrow (nBM) ( $n = 3$ ). (D) Immunoblotting of PD-L1 in AML-1 and AML-2 cells with calcitriol (400 nM) stimulation for 48 h. The densitometry analysis is shown below the bands. Immunoblotting of PD-L1 in MV-411 cells (E) and THP-1 cells (F) expressing scrambled siRNA or VDR siRNA. The uncropped blots are shown in Figure S3.



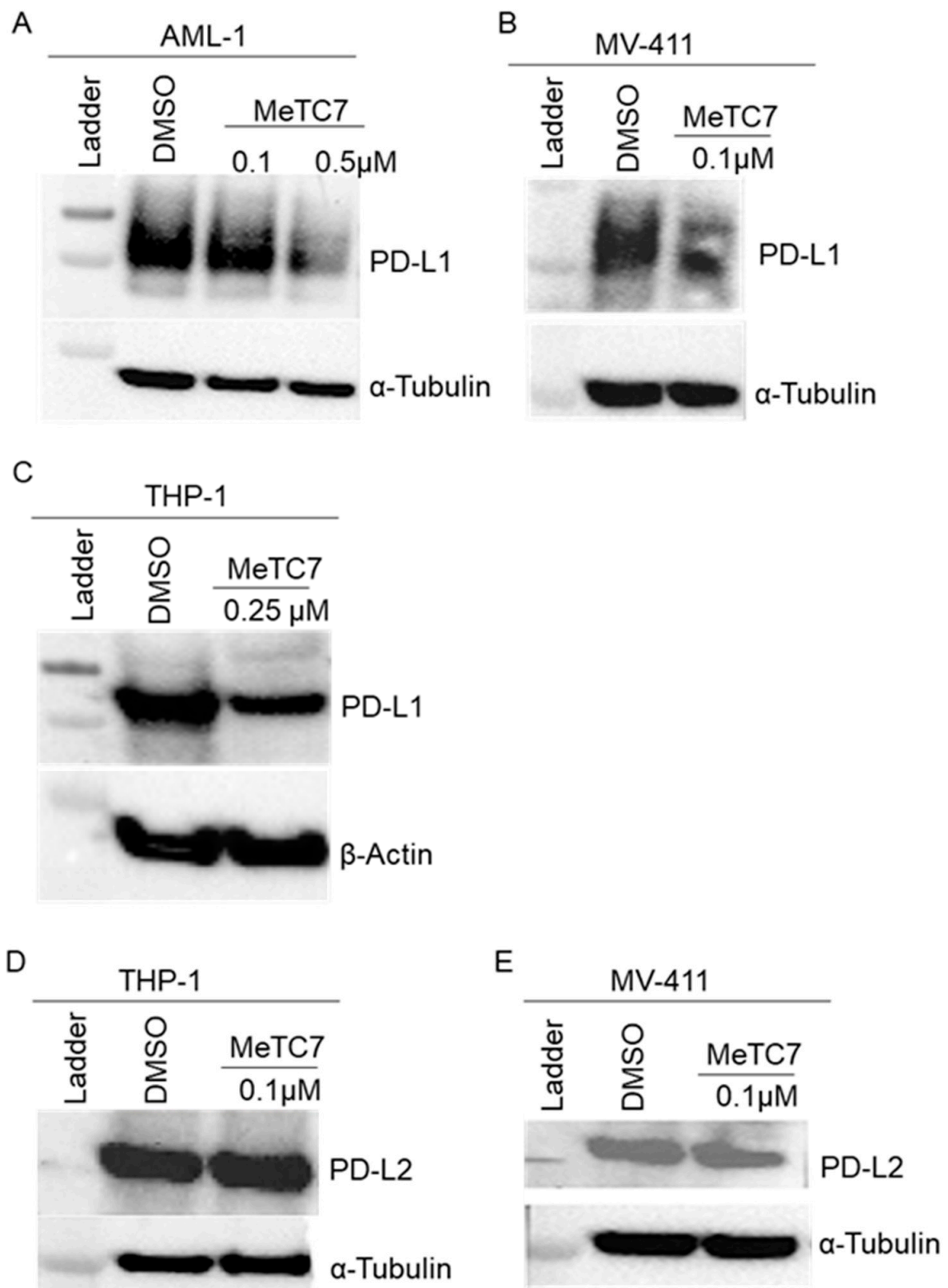
**Figure 2.** MeTC7 is a potent VDR antagonist. (A) Chemical structure of MeTC7. (B) MeTC7 demonstrates selective competitive inhibition. Heterodimerization of RXR-VDR in response to 1,25D and/or MeTC7, and homodimerization of RXR-RXR in response to bexarotene and/or MeTC7 in a mammalian 2-hybrid system (M2H). (C) VDR binding to receptor co-activator SRC1 in an M2H assay. (D) VDR binding to receptor co-activator DRIP205 in an M2H assay. (E) Selective competitive inhibition of VDR agonist 3-keto lithocholate by MeTC7. Results are plotted as ligand-mediated RXR-VDR heterodimerization (or RXR-RXR homodimerization) compared to the positive control (1,25D or bexarotene) set to 100%. The negative control is DMSO. Error bars represent standard deviations ( $* p < 0.05$  versus 1,25D control). The data are a compilation of between six and eight independent assays, with each treatment group dosed in quadruplicate for each independent assay. The transcriptional activation of the reporter gene was measured in comparison to the reference compound 1,25D or bexarotene. Error bars indicate the standard deviation of the replicate experiments. Different shadings of blue in panels B–E represent the VDR-containing M2H systems, while different shadings of green represent the RXR-only M2H. White fill represents the DMSO negative (vehicle) control.

MeTC7 treatment reduced PD-L1 expression in AML cells: Next, we investigated the effect of MeTC7 on the expression of PD-L1 and PD-L2 in primary AML and MDS cells. Effects of MeTC7 on PD-L1 and PD-L2 expression were interrogated by immunoblotting. MeTC7 (100–500 nM) treatment for 48 h reduced the expression of PD-L1 in AML-1 (Figure 3A), MV-411 (Figure 3B), and THP1 (Figure 3C) cells. Compared to MV-411 cells, MeTC7 needed a 2.5-fold higher dose (250 nM) to inhibit PD-L1 in AML cells. Further, MeTC7 treatment did not inhibit PD-L2 expression in THP-1 (Figure 3D) and MV-411 (Figure 3E) cells. Original scans of the Western blots are presented in Figure S5.

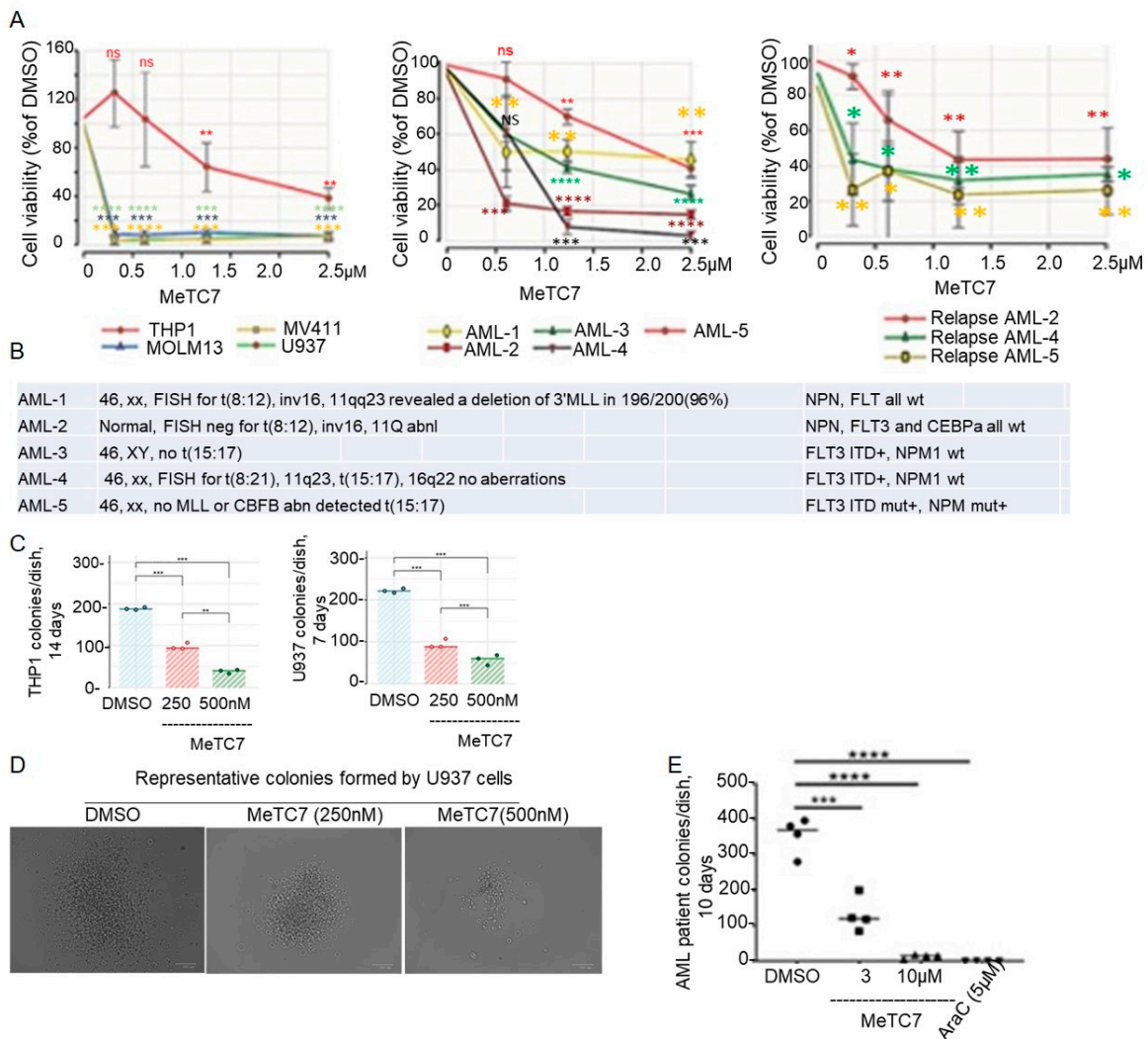
MeTC7 treatment inhibited the growth of AML cells: Treatment with MeTC7 reduced the viability of THP-1, MOLM13, MV-411, and U937 cell lines (Figure 4A) and AML cells.

Collected from five patients (Figure 4A—middle) and three relapsed patients (Figure 4A—right). The phenotypic characteristics of patients-derived AML cells used in this study are shown in Figure 4B. Next, the effect of MeTC7 treatment on the clonogenic potential of AML cell lines was investigated. MeTC7 treatment reduced the size and number of colonies formed by THP-1 (Figure 4C—left) or U937 (Figure 4C—right and Figure 4D) in a dose-dependent manner. Images (20 $\times$ ) of the U937 colonies treated with vehicle compared to MeTC7 are shown (Figure 4D). MeTC7 treatment at 10  $\mu$ M showed fewer colony units of primary AML cells, similar to Arac-C treatment, than vehicle (Figure 4E).

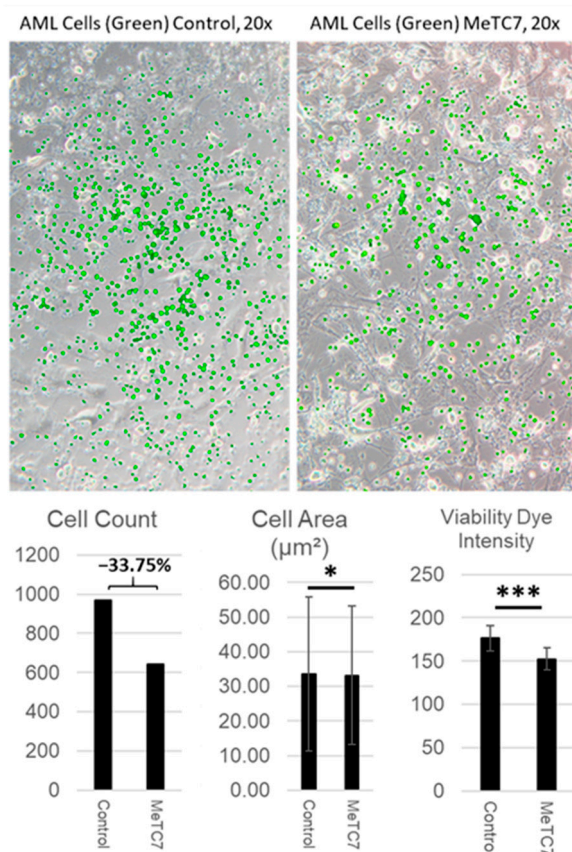




**Figure 3.** MeTC7 selectively inhibits PD-L1 expression in AML cells: MeTC7 treatment reduced PD-L1 expression in AML-1 primary cells (A), MV-411 (B), and THP-1 (C) cells during 48 h of indicated dose treatment. MeTC7 treatment at the indicated doses did not alter the expression of PD-L2 in THP-1 and MV-411 cells (D,E). The uncropped blots are shown in Figure S5.



**Figure 4.** MeTC7 inhibited the proliferation of AML cells dose dependently. MV411, THP1, U937, and MOLM13 cell lines (A—left), five randomly selected primary human AML cells (A—middle) or three relapsed AML cells (A—right) were seeded and treated with DMSO or MeTC7 in complete RPMI-1640 medium for 40 h. MTS (Promega, Celltiter96Aqueous one solution, #G3580) (10 µL) was added to each well and to those without cells (blank) and incubated for an additional 4–6 h. The optical density of the wells was recorded using the BioRad iMark microplate reader at 490 nm wavelength. The percentage viability of MeTC7-treated cells was calculated relative to DMSO-treated cells. Data as mean ± SEM are shown. (B) Table: Cytogenetic characteristics of five human primary AML cells used in Figure 5B are shown. MeTC7 treatment inhibited colonies formed by THP-1 (C—left) and U937 (C—right) cells. THP1 and U937 cells were added to MethoCult H4435 Enriched (Stem Cell Technologies, #: 04435) to achieve a concentration of 2000 cells/mL. DMSO (<0.2%) or MeTC7 (250 and 500 nM) was added. Each condition was performed in triplicate. The plates were incubated at 37 °C with 5% CO<sub>2</sub> in a humidified incubator. Colonies were counted on day 7 (U937 cells) and day 14 (THP1 cells). One-way ANOVA and Tukey’s multiple comparison tests of the number of colonies formed in control versus treatment groups were performed using GraphPrism-8. \* *p* < 0.05; \*\* *p* < 0.005, \*\*\* *p* < 0.0005, \*\*\*\* *p* < 0.00005. (D) Representative light contrast images of the U937 cell colonies treated with vehicle or MeTC7 (250 and 500 nM) on day 10 of the experiment: (C—right) growing into MethoCult H4435 enriched (Stem Cell Technologies, Canada, # 04435) are shown. (E) MeTC7 treatment reduced the colony units formed by a primary AML cell in MethoCult H4435 enriched dose dependently. Ara-C was used as a positive control. Details of the experimental procedures are described in the Supplementary Information section.

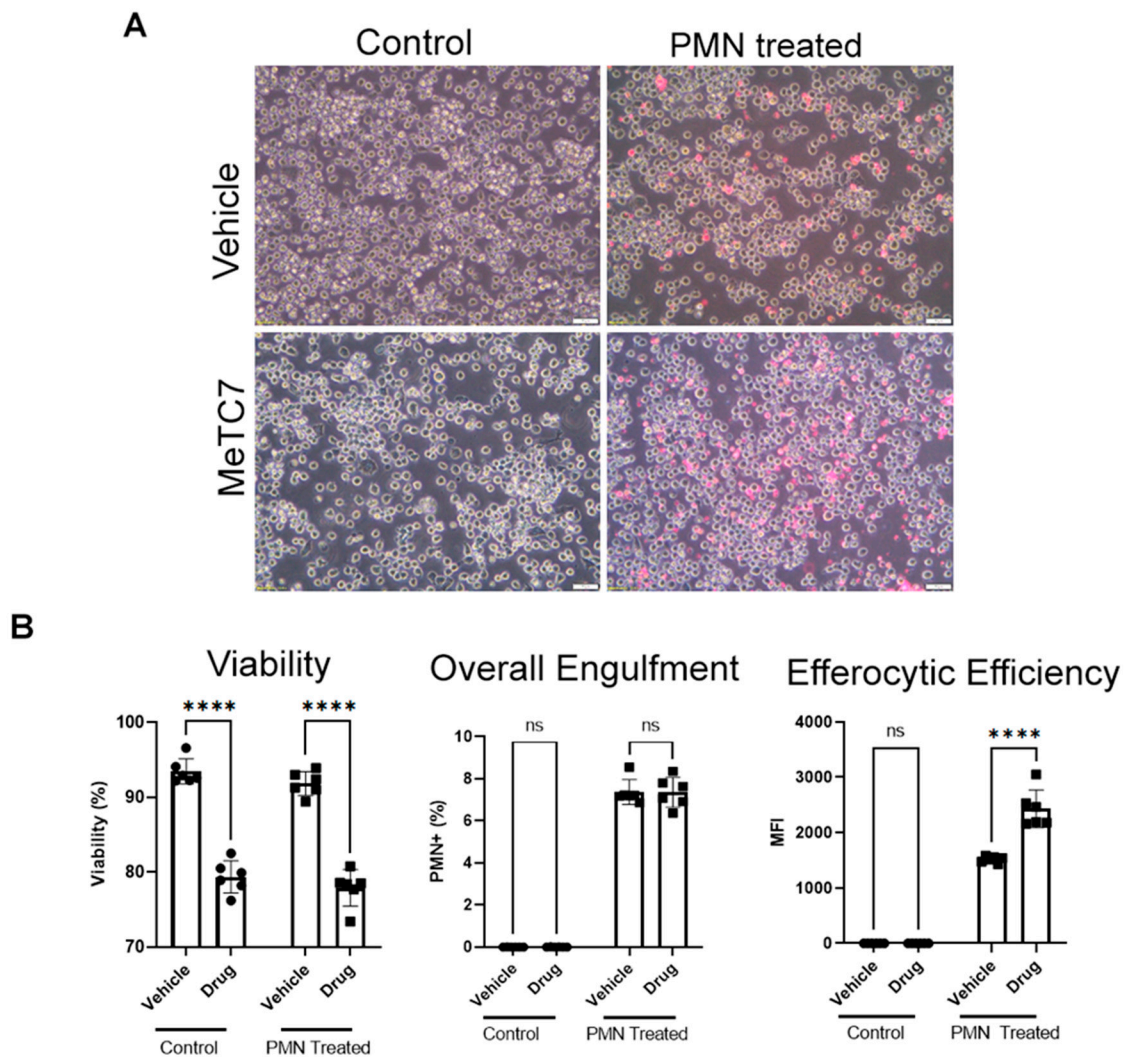


**Figure 5.** Effect of MeTC7 on the attachment of primary AML cells with MSCs. MSCs were co-cultured with pre-stained CellTracker Green for 24 h. Control (DMSO) and MeTC7 (300 nM) treatment occurred by the addition of media-containing treatment into an equal volume of co-culture-containing media. At 24 and 48 h after treatment, cells were imaged using an Olympus CKX-41 inverted microscope equipped with epifluorescence illumination and the U-FF fluorescence filter kit (excitation 467–498 nm). Image acquisition used Olympus cellSens imaging software version 2.3. Background subtracted fluorescence images were merged with brightfield images using Adobe Photoshop, release 23.2.2. Annotation for \*  $p < 0.05$  and \*\*\*  $p < 0.0005$ . For area quantification, ImageJ (Fiji) software (ImageJ 1.53t, Java 1.8.0\_322 (64-bit)) was used. Randomly selected AML cells ( $n = 400$ ) from each population were manually traced. Statistical analyses were performed using  $n = 400$  respective cell populations. Area of traced cell calculated by software was calibrated to image parameters. Cell viability (dye intensity) was determined semi-quantitatively utilizing the color expression via the reciprocal intensity of images using ImageJ (ImageJ 1.53t, Java 1.8.0\_322 (64-bit)).

MeTC7 prevents AML adhered to MSCs: MSCs support the survival and proliferation of primary human AML cells [28]. Co-culture of AML-MSCs was shown to enhance the proliferation of AML cells, as well as chemoresistance [28]. We employed an AML-MSC co-culture method to investigate whether MeTC7 treatment could block adherence of primary AML cells with MSCs. MeTC7 treatment, under co-culture conditions with MSCs, significantly reduced cell counts, sizes, and viability of primary AML adhered with MSCs (Figure 5). MeTC7 suppressed AML cell viabilities selectively without affecting the viability of MSCs.

MeTC7 augments the efferocytotic efficiency of THP1 cells: Phagocytosis of dead and dying cells, also termed efferocytosis, is essential for tissue homeostasis and maintenance [29]. Defective efferocytosis underlies the causes of a growing list of inflammatory diseases [30]. Blockade of PD-1/PD-L1 in vivo has been shown to increase macrophage efferocytosis [31]. We examined if VDR/PD-L1 inhibition by MeTC7 could affect the efferocytotic efficiency of THP-1 macrophages by measuring repeated efferocytotic activity (Figure 6A).

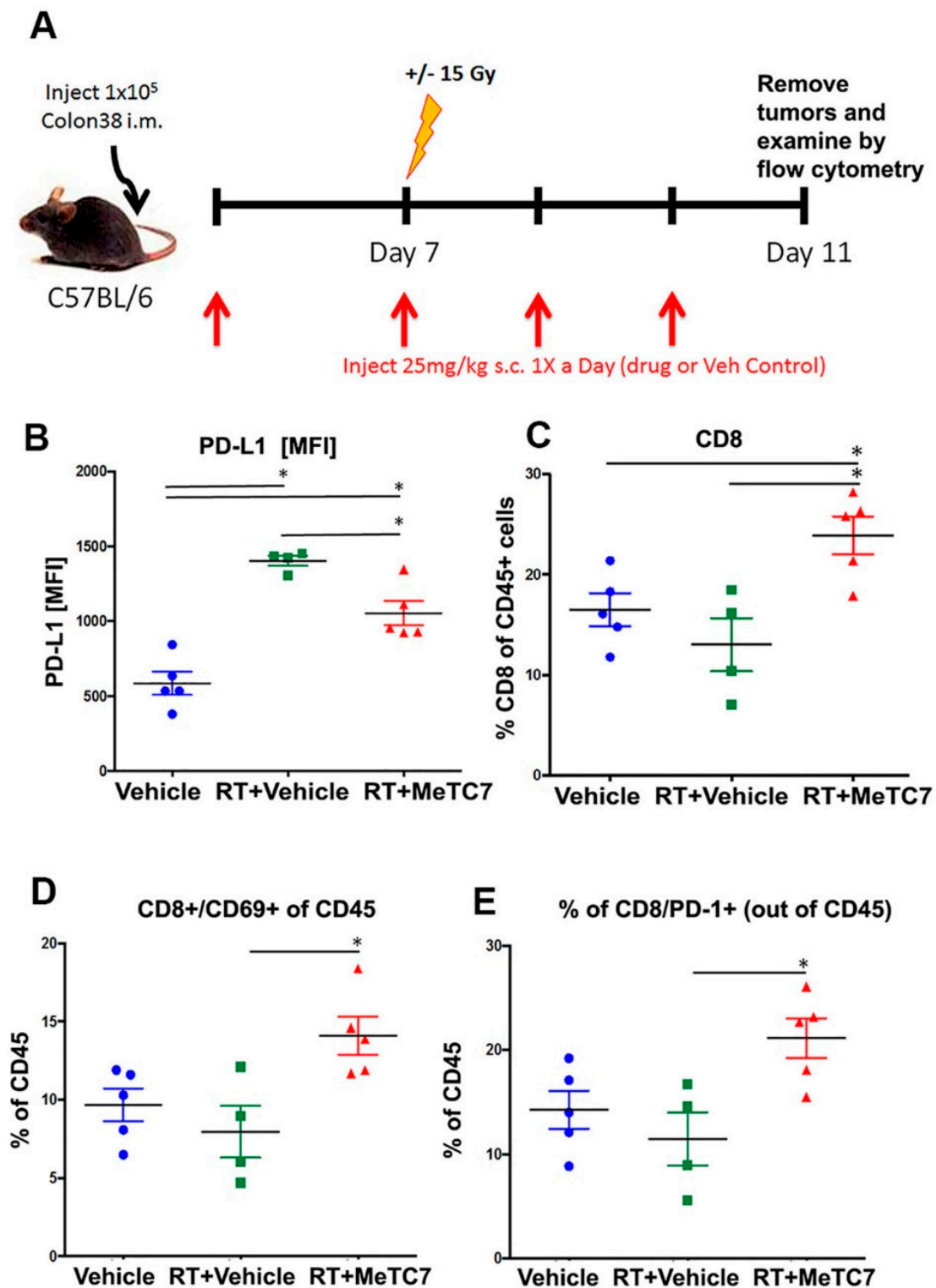
MeTC7 treatment increased the efferocytic efficiency of THP-1 cells (Figure 6B, right), while the total engulfment was not increased (Figure 6B, middle) after MeTC7 treatment.



**Figure 6.** MeTC7 enhances the phagocytotic activity of THP1 cells. THP1 cells were treated with MeTC7 (340 nM) or vehicle for 48 h. Neutrophils (PMNs), isolated from human peripheral blood, were incubated at  $-80^{\circ}\text{C}$  in FBS+ 10% DMSO for 24 h to induce apoptosis. Apoptotic neutrophils were washed with PBS and fluorescently labeled with  $2\ \mu\text{M}$  PKH26GL. End-stage neutrophils were provided in excess (10:1) to plated THP1 cells for 3 h. Cells were imaged and collected for flow cytometry analysis. All samples were run on an LSRII flow cytometer using FSC, SSC, 355 nm (DAPI), and 535 nm (PKH26). Analysis was performed using FlowJo version 10.7.1. Annotation for ns: not significant, \*\*\*\*  $p < 0.0001$ . Images were taken at  $20\times$ . Scale bar =  $50\ \mu\text{M}$ .

MeTC7 inhibits radiotherapy (RT)-induced PD-L1 expression in vivo: MC38 colorectal cancer cell-based syngeneic animal model [26] in which VDR and PD-L1 overexpression co-occurs under radiation therapy was employed to estimate the efficacy of MeTC7. The treatment of MC38 colorectal cancer cell-derived tumors (Schema: Figure 7A) with MeTC7 growing in mice showed that MeTC7, in combination with RT, significantly reduced the surface expression of PD-L1 on tumor cells (Figure 7B). In addition, MeTC7 treatment in combination with RT increased CD8+T-cell infiltration (Figure 7C), and the percent of CD8+ T cells expressing CD69 and PD-1 activation markers increased compared to vehicle or RT + vehicle (Figure 7D,E).



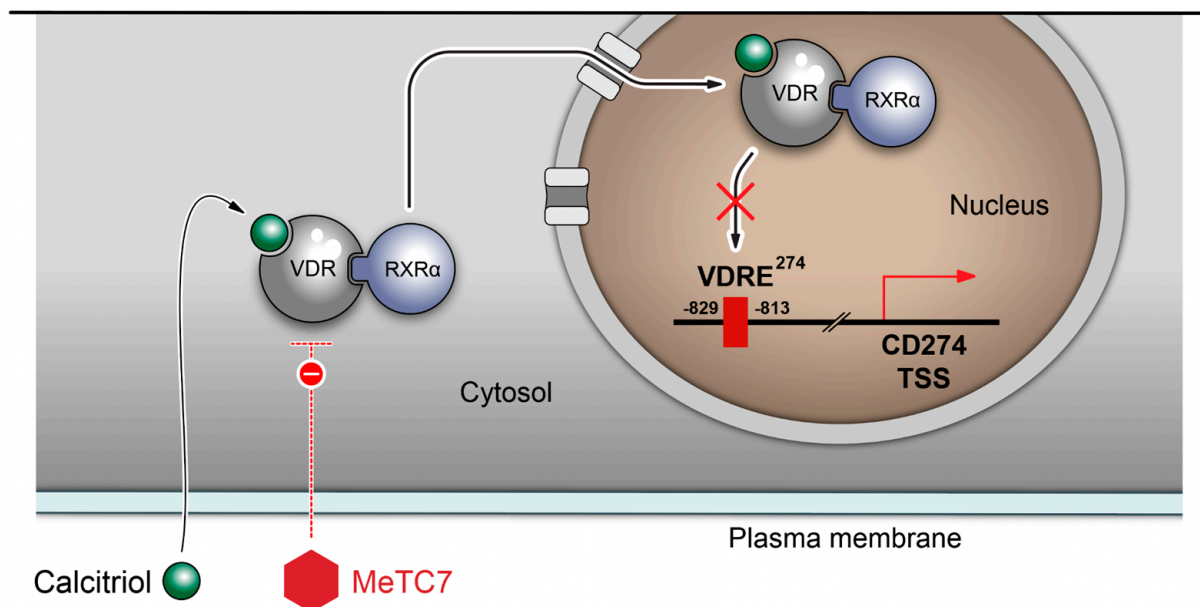


**Figure 7.** MeTC7 reduces PD-L1 expression in an RT-inducible PD-L1 overexpression syngeneic model. (A): Schema of determination of activity against PD-L1 activated by RT in an orthotopic model of MC38 colorectal cancer in BL7 mice. MeTC7, in combination with RT-abrogated RT-induced PD-L1 activation in CD45<sup>+</sup> tumor cells post-RT (B); (C), increased CD8<sup>+</sup>-T-cell infiltration in tumors significantly compared to vehicle or RT + vehicle. (D,E): MeTC7 increased the % of cells expressing CD69 (D) and PD-1 (E) compared to vehicle and vehicle + RT. The details of the antibodies used are listed in Supplementary Information S1. Annotation for \*  $p < 0.05$ .



#### 4. Discussion

Our study provides a small-molecule MeTC7 that can inhibit PD-L1 expression in AML (Figure 3). Development of MeTC7 as the inhibitor of VDR/PD-L1 assumes importance in the context of calcitriol's role in the upregulation of PD-L1 (Figure 8), enrichment of Tregs [32], suppressions of CD8+T cells [33], and stunting of NK cell growth [34] and T-cell activation [35], each of which can be exploited by tumors to evade immune detection. MeTC7 selectively reduces PD-L1 in AML cell lines, sparing PD-L2 (Figure 3D,E). Both PD-L1 and PD-L2 compete for binding with the PD-1 receptor with similar affinity. Lack of activity against PD-L2 is desirable because PD-L2 is associated with the functions of macrophages, DCs, mast cells, and vascular endothelial cells and plays critical roles in normal immunity. To validate the anti-PD-L1 effects of MeTC7 *in vivo*, we utilized a syngeneic colon cancer model in which radiation therapy (RT) induces overexpression of both VDR and PD-L1 on tumor cells. Although MeTC7 initially slowed the growth of AML xenograft in NSG mice (Figure S6) despite starting at higher average volume sizes, the RT-based model was considered more informative because of the convergence of VDR and PD-L1 and the presence of the intact immune system. In this model, MeTC7 reduced PD-L1 expression and increased lymphoid activation marker CD69+ on CD8+ T-cell populations in the tumors, consistent with PD-L1/PD-1 pathway blockade.



**Figure 8.** Proposed signaling effects of MeTC7 against VDR/PD-L1 in cancer cells.

MeTC7 is both structurally and mechanistically different from BMS202 (and analogs), CA-170, and INCB086550, the other leading small molecules that were shown to target the PD-L1/PD-1 axis. BMS202 and INCB086550 block PD-L1/PD-1 interactions, mimicking the therapeutic actions of antibodies [18,20–23]. MeTC7 inhibits surface and intracellular PD-L1. Given the potential of MeTC7 in inhibiting PD-L1, it was considered important to validate that MeTC7 was free from any residual VDR agonistic effects. The literature described antagonists carrying partial VDR agonistic effects, which can overexpress PD-L1. M2H assay showed that MeTC7 not only demonstrated specific VDR inhibition when combined with calcitriol but also did not compete nor bind with non-VDR receptors like RXR under any of the concentrations tested (Figure 2). Heterodimerization of VDR with transcriptional coactivators SRC1 and DRIP205 was also effectively inhibited by MeTC7.

The rationale for targeting PD-L1 in AML stems from: (1) overexpression of PD-L1 in AML and MDS, the precursor of AML, and their association with poor prognosis (Figure S1) [36,37]; (2) PD-L1 enrichment in AML blasts at post-transplantation relapse; (3) PD-L1 orchestrated AML relapses after allogeneic hematopoietic cell transplantation

(allo-HCT) [38] and (4) PD-L1 induced secondary resistance to hypomethylating agents (HMAs) in AML [39]. MeTC7 can also be effective in enhancing the response of HMAs to both AML and its precursor neoplasm, MDS since HMAs increase PD-L1 expression in MDS and AML. The activity of anti-PD-L1 antibodies among AML patients and those with relapsed disease was shown [40]. Among AML subtypes, *inv(16)/t(16;16)*, *t(11q23)/MLL*, and AML complex, which exhibit VDR mRNA overexpression (Figure 1A) and can be targeted by MeTC7. VDR/PD-L1 inhibition by MeTC7 results in loss of viability and colony formation capabilities of primary and relapsed AML cells.

Further, our studies show that targeting the VDR/PD-L1 axis prevents AML cells' attachment to MSCs (Figure 5). Interactions of AML/MSCs and MDS/MSC cells enable MDS and AML's genesis, progression, chemoresistance, and relapse [41,42]. Further, MeTC7 treatment can enhance the phagocytotic activities [43] of macrophages (Figure 6). Defective efferocytosis is one of the underlying causes of malignancies [44,45]. Efferocytosis of apoptotic neutrophils by macrophages was shown to promote anti-inflammatory signaling, prevent neutrophil lysis, and dampening of immune responses [46]. Similarly, tumor intrinsic and intracellular PD-L1 signals enhance cancer cell survival and confer resistance to anti-PD-1/PD-L1 antibody therapies [47]. Silencing PD-L1 in MDA-MB-231 breast cancer cells increased apoptosis and enhanced susceptibility to doxorubicin *in vitro* and *in vivo* [48]. Similarly, CRISPR/Cas9 knockout of PD-L1 enhanced the sensitivity of human osteosarcoma cells to doxorubicin and paclitaxel and blocked the ability to form three-dimensional spheroids *in vitro* [49].

Potential clinical applications of this study and specifically of MeTC7 reside in the small-molecule immunotherapy of AML, ovarian cancer, and pancreatic cancer, the cell lines of which show vitamin D/VDR dependencies of PD-L1 expressions.

A major limitation of this study is the lack of an *in vivo* AML model that can recapitulate the vitamin D/VDR/PD-L1 axis, which would validate the above-shown outcomes of MeTC7 treatment in the AML tumor microenvironment.

## 5. Conclusions

Taken together, based on the inhibitions of AML cell viability, colonies formed and PD-L1 expression, and increased phagocytosis, we anticipate that MeTC7 can improve the survival in AML via inhibition of PD-L1. Inhibition of tumor intrinsic and intracellular PD-L1 by MeTC7 would prevent PD-L1 rebound on the tumor cell surface and block the emergence of resistance. In conclusion, MeTC7 presents as a promising small molecule to inhibit PD-L1 *in vitro* and *in vivo*.

**Supplementary Materials:** The following supporting information can be downloaded at: <https://www.mdpi.com/article/10.3390/cancers15133432/s1>, Experimental methods for cell viability, Colony formation unit assay, siRNA knockdown, Chromatin Immunoprecipitation (CHIP) assay, Co-culture of mesenchymal stem cells with primary AML cells, Information about antibodies used in this study. In addition, the following figures are provided. Figure S1: PD-L1 overexpression indicates increased mortalities among AML patients. Figure S2: Vitamin DR/VDR transcriptionally regulates PD-L1 in AML and MDS cells. Figure S3: Original and unaltered full scans of Western blots presented in Figure 1C–E. Figure S4: Role of STAT3 signaling in AML cell lines. Figure S5: Original and unaltered full scans of the Western blots presented in Figure 3A–E. Figure S6: Antitumor activity of MeTC7 in U937 cell-derived xenograft model.

**Author Contributions:** R.K.S. conceived and organized the studies and brought partial resources through TDF and CTSA pilot awards in team with S.A.G., D.C.L. and R.G.M.; N.K., N.A.S., T.M., J.P.M., J.N.H., N.Z., A.M., K.K.K., C.W.A.S., D.P. and P.S. contributed to MTS assay, siRNA, cell culture, drug treatment, pcr and Western blots, image analysis and data analysis, manuscript writing and editing; M.Y., Y.T., T.G. and H.M. performed the CHIP assay. E.R.Q. measured efferocytic activity; H.K., D.M.S., M.W.B., L.M.C., Y.K. and J.L. contributed through colony formation assays, flow cytometry and provision for resources such as AML cell lines, primary and relapsed AML cells and manuscript data analysis, and supervision and editing for those data; T.C. and O.A. contributed through transmigration assay; N.Y. contributed shRNA/siRNA experiment, J.H. and S.R. performed

all M2H assays under supervision of P.W.J. M.K.K. analyzed the chemical structure and purity of MeTC7; A.S.Z., E.D.T., critically reviewed the data, participated in manuscript assembly; A.S., and N.V.D. performed in-silico docking experiments; N.R. attempted MeTC7-VDR co-crystallizations; N.V.D., R.B.R.-T., J.L., M.W.B., L.M.C., E.D.T., S.A.G., D.C.L., P.W.J. and R.G.M. reviewed the data, provided key resources, and edited the manuscript. All authors have read and agreed to the published version of the manuscript.

**Funding:** This research was funded by the University of Rochester CTSA award number UL1 TR002001, from the National Center for Advancing Translational Sciences of the National Institutes of Health, and the Technology Development Fund of the University of Rochester award to R.K.S., S.G., D.L., and R.M. N.V.D. acknowledges following funding: National Institutes of Health, Grant/Award Numbers: R35 GM134864, 1RF1 AG071675-01, 1R01 AT012053; Passan Foundation; National Science Foundation, Grant/Award Number: 2210963. The funders had no role in the design of the study; in the collection, analyses, or interpretation of data; in the writing of the manuscript, or in the decision to publish the results.

**Institutional Review Board Statement:** All experiments involving human samples were approved by the University of Rochester institutional committee. Approval numbers are: RSRB 17981 (study 0043), approved 21 November 2022, and RSRB ULEU07047 (study 20123), approved 3 May 2022. All the methods were performed with complete adherence to the relevant guidelines and regulations.

**Informed Consent Statement:** Written informed consent for publication was obtained from participating AML patients and healthy donors.

**Data Availability Statement:** Raw data will be provided upon reasonable request.

**Acknowledgments:** Michael Conley is acknowledged for image analyses (Figure 5).

**Conflicts of Interest:** R.K.S. and R.G.M. are listed as the co-inventors on U.S. (11,034,719), EU (3128996), and Canadian (2,982,270) patents assigned to the University of Rochester. The rest of the authors do not carry a conflict of interest.

## References

1. Dong, H.; Zhu, G.; Tamada, K.; Chen, L. B7-H1, a third member of the B7 family, co-stimulates T-cell proliferation and interleukin-10 secretion. *Nat. Med.* **1999**, *5*, 1365–1369. [[CrossRef](#)] [[PubMed](#)]
2. Dong, H.; Strome, S.E.; Salomao, D.R.; Tamura, H.; Hirano, F.; Flies, D.B.; Roche, P.C.; Lu, J.; Zhu, G.; Tamada, K.; et al. Tumor-associated B7-H1 promotes T-cell apoptosis: A potential mechanism of immune evasion. *Nat. Med.* **2002**, *8*, 793–800. [[CrossRef](#)] [[PubMed](#)]
3. Vandenborre, K.; Van Gool, S.W.; Kasran, A.; Ceuppens, J.L.; Boogaerts, M.A.; Vandenberghe, P. Interaction of CTLA-4 (CD152) with CD80 or CD86 inhibits human T-cell activation. *Immunology* **1999**, *98*, 413–421. [[CrossRef](#)] [[PubMed](#)]
4. ElTanbouly, M.A.; Schaafsma, E.; Noelle, R.J.; Lines, J.L. VISTA: Coming of age as a multi-lineage immune checkpoint. *Clin. Exp. Immunol.* **2020**, *200*, 120–130. [[CrossRef](#)] [[PubMed](#)]
5. Lamberti, G.; Sisi, M.; Andrini, E.; Palladini, A.; Giunchi, F.; Lollini, P.L.; Ardizzoni, A.; Gelsomino, F. The mechanisms of PD-L1 regulation in non-small-cell lung cancer (NSCLC): Which are the involved players? *Cancers* **2020**, *12*, 3129. [[CrossRef](#)]
6. Zhang, W.; Pang, Q.; Yan, C.; Wang, Q.; Yang, J.; Yu, S.; Liu, X.; Yuan, Z.; Wang, P.; Xiao, Z. Induction of PD-L1 expression by epidermal growth factor receptor-mediated signaling in esophageal squamous cell carcinoma. *OncoTargets Ther.* **2017**, *10*, 763–771. [[CrossRef](#)]
7. Dimitrov, V.; Bouttier, M.; Boukhaled, G.; Salehi-Tabar, R.; Avramescu, R.G.; Memari, B.; Hasaj, B.; Lukacs, G.L.; Krawczyk, C.M.; White, J.H. Hormonal vitamin D up-regulates tissue-specific PD-L1 and PD-L2 surface glycoprotein expression in humans but not mice. *J. Biol. Chem.* **2017**, *292*, 20657–20668. [[CrossRef](#)]
8. Cao, D.; Qi, Z.; Pang, Y.; Li, H.; Xie, H.; Wu, J.; Huang, Y.; Zhu, Y.; Shen, Y.; Zhu, Y.; et al. Retinoic acid-related orphan receptor C regulates proliferation, glycolysis, and chemoresistance via the PD-L1/ITGB6/STAT3 signaling axis in bladder cancer. *Cancer Res.* **2019**, *79*, 2604–2618. [[CrossRef](#)]
9. Antonangeli, F.; Natalini, A.; Garassino, M.C.; Sica, A.; Santoni, A.; Di Rosa, F. Regulation of PD-L1 Expression by NF- $\kappa$ B in Cancer. *Front. Immunol.* **2020**, *11*, 584626. [[CrossRef](#)]
10. Garcia-Diaz, A.; Shin, D.S.; Moreno, B.H.; Saco, J.; Escuin-Ordinas, H.; Rodriguez, G.A.; Zaretsky, J.M.; Sun, L.; Hugo, W.; Wang, X.; et al. Interferon receptor signaling pathways regulating PD-L1 and PD-L2 expression. *Cell Rep.* **2017**, *19*, 1189–1201. [[CrossRef](#)]
11. Brahmer, J.R.; Tykodi, S.S.; Chow, L.Q.; Hwu, W.J.; Topalian, S.L.; Hwu, P.; Drake, C.G.; Camacho, L.H.; Kauh, J.; Odunsi, K.; et al. Safety and activity of anti-PD-L1 antibody in patients with advanced cancer. *N. Engl. J. Med.* **2012**, *366*, 2455–2465. [[CrossRef](#)]
12. Jiang, X.; Wang, J.; Deng, X.; Xiong, F.; Ge, J.; Xiang, B.; Wu, X.; Ma, J.; Zhou, M.; Li, X.; et al. Role of the tumor microenvironment in PD-L1/PD-1-mediated tumor immune escape. *Mol. Cancer* **2019**, *18*, 10. [[CrossRef](#)]

13. Koustas, E.; Sarantis, P.; Papavassiliou, A.G.; Karamouzis, M.V. The resistance mechanisms of checkpoint inhibitors in solid tumors. *Biomolecules* **2020**, *10*, 666. [[CrossRef](#)] [[PubMed](#)]
14. Escors, D.; Gato-Cañas, M.; Zuazo, M.; Arasanz, H.; García-Granda, M.J.; Vera, R.; Kochan, G. The intracellular signalosome of PD-L1 in cancer cells. *Signal Transduct. Target. Ther.* **2018**, *3*, 26. [[CrossRef](#)]
15. Chen, G.; Huang, A.C.; Zhang, W.; Zhang, G.; Wu, M.; Xu, W.; Yu, Z.; Yang, J.; Wang, B.; Sun, H.; et al. Exosomal PD-L1 contributes to immunosuppression and is associated with anti-PD-1 response. *Nature* **2018**, *560*, 382–386. [[CrossRef](#)] [[PubMed](#)]
16. Poggio, M.; Hu, T.; Pai, C.C.; Chu, B.; Belair, C.D.; Chang, A.; Montabana, E.; Lang, U.E.; Fu, Q.; Fong, L.; et al. Suppression of exosomal PD-L1 induces systemic anti-tumor immunity and memory. *Cell* **2019**, *177*, 414–427.e13. [[CrossRef](#)]
17. Gong, B.; Kiyotani, K.; Sakata, S.; Nagano, S.; Kumehara, S.; Baba, S.; Besse, B.; Yanagitani, N.; Friboulet, L.; Nishio, M.; et al. Secreted PD-L1 variants mediate resistance to PD-L1 blockade therapy in non-small cell lung cancer. *J. Exp. Med.* **2019**, *216*, 982–1000. [[CrossRef](#)] [[PubMed](#)]
18. Yamaguchi, H.; Hsu, J.M.; Yang, W.H.; Hung, M.C. Mechanisms regulating PD-L1 expression in cancers and associated opportunities for novel small-molecule therapeutics. *Nat. Rev. Clin. Oncol.* **2022**, *19*, 287–305. [[CrossRef](#)] [[PubMed](#)]
19. Ramos-Casals, M.; Brahmer, J.R.; Callahan, M.K.; Flores-Chávez, A.; Keegan, N.; Khamashta, M.A.; Lambotte, O.; Mariette, X.; Prat, A.; Suárez-Almazor, M.E. Immune-related adverse events of checkpoint inhibitors. *Nat. Rev. Dis. Primers.* **2020**, *6*, 38. [[CrossRef](#)] [[PubMed](#)]
20. Koblisch, H.K.; Wu, L.; Wang, L.S.; Liu, P.C.C.; Wynn, R.; Rios-Doria, J.; Spitz, S.; Liu, H.; Volgina, A.; Zolotarjova, N.; et al. Characterization of INCB086550: A potent and novel small-molecule PD-L1 inhibitor. *Cancer. Discov.* **2022**, *12*, 1482–1499. [[CrossRef](#)]
21. Skalniak, L.; Zak, K.M.; Guzik, K.; Magiera, K.; Musielak, B.; Pachota, M.; Szelazek, B.; Kocik, J.; Grudnik, P.; Tomala, M.; et al. Small-molecule inhibitors of PD-1/PD-L1 immune checkpoint alleviate the PD-L1-induced exhaustion of T-cells. *Oncotarget* **2017**, *8*, 72167–72181. [[CrossRef](#)] [[PubMed](#)]
22. Guzik, K.; Zak, K.M.; Grudnik, P.; Magiera, K.; Musielak, B.; Törner, R.; Skalniak, L.; Dömling, A.; Dubin, G.; Holak, T.A. Small-molecule inhibitors of the programmed cell death-1/programmed death-ligand 1 (PD-1/PD-L1) Interaction via transiently induced protein states and dimerization of PD-L1. *J. Med. Chem.* **2017**, *60*, 5857–5867. [[CrossRef](#)] [[PubMed](#)]
23. Musielak, B.; Kocik, J.; Skalniak, L.; Magiera-Mularz, K.; Sala, D.; Czub, M.; Stec, M.; Siedlar, M.; Holak, T.A.; Plewka, J. CA-170—A potent small-molecule PD-L1 inhibitor or not? *Molecules* **2019**, *24*, 2804. [[CrossRef](#)] [[PubMed](#)]
24. Khazan, N.; Kim, K.K.; Hansen, J.N.; Singh, N.A.; Moore, T.; Snyder, C.W.A.; Pandita, R.; Strawderman, M.; Fujihara, M.; Takamura, Y.; et al. Identification of a Vitamin-D Receptor antagonist, MeTC7, which inhibits the growth of xenograft and transgenic tumors in vivo. *J. Med. Chem.* **2022**, *65*, 6039–6055. [[CrossRef](#)]
25. Azadniv, M.; Myers, J.R.; McMurray, H.R.; Guo, N.; Rock, P.; Coppage, M.L.; Ashton, J.; Becker, M.W.; Calvi, L.M.; Liesveld, J.L. Bone marrow mesenchymal stromal cells from acute myelogenous leukemia patients demonstrate adipogenic differentiation propensity with implications for leukemia cell support. *Leukemia* **2020**, *34*, 391–403. [[CrossRef](#)]
26. Connolly, K.A.; Belt, B.A.; Figueroa, N.M.; Murthy, A.; Patel, A.; Kim, M.; Lord, E.M.; Linehan, D.C.; Gerber, S.A. Increasing the efficacy of radiotherapy by modulating the CCR2/CCR5 chemokine axes. *Oncotarget* **2016**, *7*, 86522–86535. [[CrossRef](#)]
27. Benekli, M.; Xia, Z.; Donohue, K.A.; Ford, L.A.; Pixley, L.A.; Baer, M.R.; Baumann, H.; Wetzler, M. Constitutive activity of signal transducer and activator of transcription 3 protein in acute myeloid leukemia blasts is associated with short disease-free survival. *Blood* **2002**, *99*, 252–257. [[CrossRef](#)]
28. Brenner, A.K.; Nepstad, I.; Bruserud, Ø. Mesenchymal stem cells support survival and proliferation of primary human acute myeloid leukemia cells through heterogeneous molecular mechanisms. *Front. Immunol.* **2017**, *8*, 106. [[CrossRef](#)]
29. Arandjelovic, S.; Ravichandran, K.S. Phagocytosis of apoptotic cells in homeostasis. *Nat. Immunol.* **2015**, *16*, 907–917. [[CrossRef](#)]
30. Kawano, M.; Nagata, S. Efferocytosis and autoimmune disease. *Int. Immunol.* **2018**, *30*, 551–558. [[CrossRef](#)]
31. Gordon, S.R.; Maute, R.L.; Dulken, B.W.; Hutter, G.; George, B.M.; McCracken, M.N.; Gupta, R.; Tsai, J.M.; Sinha, R.; Corey, D.; et al. PD-1 expression by tumour-associated macrophages inhibits phagocytosis and tumour immunity. *Nature* **2017**, *545*, 495–499. [[CrossRef](#)] [[PubMed](#)]
32. Fisher, S.A.; Rahimzadeh, M.; Brierley, C.; Gratton, B.; Doree, C.; Kimber, C.E.; Cajide, A.P.; Lamikanra, A.A.; Roberts, D.J. The role of vitamin D in increasing circulating T regulatory cell numbers and modulating T regulatory cell phenotypes in patients with inflammatory disease or in healthy volunteers: A systematic review. *PLoS ONE.* **2019**, *14*, e0222313. [[CrossRef](#)]
33. Cantorna, M.T. Why do T cells express the vitamin D receptor? *Ann. N. Y. Acad. Sci.* **2011**, *1217*, 77–82. [[CrossRef](#)]
34. Cantorna, M.T.; Snyder, L.; Lin, Y.D.; Yang, L. Vitamin D and 1,25(OH)2D regulation of T cells. *Nutrients* **2015**, *7*, 3011–3021. [[CrossRef](#)] [[PubMed](#)]
35. von Essen, M.R.; Kongsbak, M.; Schjerling, P.; Olgaard, K.; Odum, N.; Geisler, C. Vitamin D controls T cell antigen receptor signaling and activation of human T cells. *Nat. Immunol.* **2010**, *11*, 344–349. [[CrossRef](#)] [[PubMed](#)]
36. Brodská, B.; Otevřelová, P.; Šálek, C.; Fuchs, O.; Gašová, Z.; Kuželová, K. High PD-L1 expression predicts for worse outcome of leukemia patients with concomitant NPM1 and FLT3 Mutations. *Int. J. Mol. Sci.* **2019**, *20*, 2823. [[CrossRef](#)]
37. Dong, Y.; Han, Y.; Huang, Y.; Jiang, S.; Huang, Z.; Chen, R.; Yu, Z.; Yu, K.; Zhang, S. PD-L1 Is expressed and promotes the expansion of regulatory T cells in acute myeloid leukemia. *Front. Immunol.* **2020**, *11*, 1710. [[CrossRef](#)]



38. Toffalori, C.; Zito, L.; Gambacorta, V.; Riba, M.; Oliveira, G.; Bucci, G.; Barcella, M.; Spinelli, O.; Greco, R.; Crucitti, L.; et al. Immune signature drives leukemia escape and relapse after hematopoietic cell transplantation. *Nat. Med.* **2019**, *25*, 603–611. [[CrossRef](#)]
39. Daver, N.; Garcia-Manero, G.; Basu, S.; Boddu, P.C.; Alfayez, M.; Cortes, J.E.; Konopleva, M.; Ravandi-Kashani, F.; Jabbour, E.; Kadia, T.; et al. Efficacy, safety, and biomarkers of response to azacitidine and nivolumab in relapsed/refractory acute myeloid leukemia: A nonrandomized, open-label, phase II study. *Cancer Discov.* **2019**, *9*, 370–383. [[CrossRef](#)]
40. Ghosh, A.; Barba, P.; Perales, M.A. Checkpoint inhibitors in AML: Are we there yet? *Br. J. Haematol.* **2020**, *188*, 159–167. [[CrossRef](#)]
41. Waclawiczek, A.; Hamilton, A.; Rouault-Pierre, K.; Abarrategi, A.; Albornoz, M.G.; Miraki-Moud, F.; Bah, N.; Gribben, J.; Fitzgibbon, J.; Taussig, D.; et al. Mesenchymal niche remodeling impairs hematopoiesis via stanniocalcin 1 in acute myeloid leukemia. *J. Clin. Investig.* **2020**, *130*, 3038–3050. [[CrossRef](#)] [[PubMed](#)]
42. von der Heide, E.K.; Neumann, M.; Vosberg, S.; James, A.R.; Schroeder, M.P.; Ortiz-Tanchez, J.; Isaakidis, K.; Schlee, C.; Luther, M.; Jöhrens, K.; et al. Molecular alterations in bone marrow mesenchymal stromal cells derived from acute myeloid leukemia patients. *Leukemia* **2016**, *31*, 1069–1078. [[CrossRef](#)]
43. Querfeld, U. Vitamin D and inflammation. *Pediatr. Nephrol.* **2013**, *28*, 605–610. [[CrossRef](#)] [[PubMed](#)]
44. Doran, A.C.; Yurdagul, A.; Tabas, I. Efferocytosis in health and disease. *Nat. Rev. Immunol.* **2020**, *20*, 254–267. [[CrossRef](#)]
45. Mehrotra, P.; Ravichandran, K.S. Drugging the efferocytosis process: Concepts and opportunities. *Nat. Rev. Drug Discov.* **2022**, *21*, 601–620. [[CrossRef](#)] [[PubMed](#)]
46. Greenlee-Wacker, M.C. Clearance of apoptotic neutrophils and resolution of inflammation. *Immunol. Rev.* **2016**, *273*, 357–370. [[CrossRef](#)]
47. Padmanabhan, S.; Zou, Y.; Vancurova, I. Immunoblotting analysis of intracellular PD-L1 levels in interferon- $\gamma$ -treated ovarian cancer cells stably transfected with Bcl3 shRNA. *Methods Mol. Biol.* **2020**, *2108*, 211–220. [[CrossRef](#)]
48. Ghebeh, H.; Lehe, C.; Barhoush, E.; Al-Romaih, K.; Tulbah, A.; Al-Alwan, M.; Hendrayani, S.F.; Manogaran, P.; Alaiya, A.; Al-Tweigeri, T.; et al. Doxorubicin downregulates cell surface B7-H1 expression and upregulates its nuclear expression in breast cancer cells: Role of B7-H1 as an anti-apoptotic molecule. *Breast Cancer Res.* **2010**, *12*, R48. [[CrossRef](#)]
49. Liao, Y.; Chen, L.; Feng, Y.; Shen, J.; Gao, Y.; Cote, G.; Choy, E.; Harmon, D.; Mankin, H.; Hornicek, F.; et al. Targeting programmed cell death ligand 1 by CRISPR/Cas9 in osteosarcoma cells. *Oncotarget* **2017**, *8*, 30276–30287. [[CrossRef](#)]

**Disclaimer/Publisher’s Note:** The statements, opinions and data contained in all publications are solely those of the individual author(s) and contributor(s) and not of MDPI and/or the editor(s). MDPI and/or the editor(s) disclaim responsibility for any injury to people or property resulting from any ideas, methods, instructions or products referred to in the content.